Anomalous Thermal Hysteresis in Magnetization and Resistivity of $La_{1-x}Sr_xMnO_3$

Joonghoe Dho, W. S. Kim, and N. H. Hur*

Center for CMR Materials, Korea Research Institute of Standards and Science, Yusong, P.O. Box 102, Taejon 305-600, Korea

(Received 12 June 2001; published 10 October 2001)

We have investigated thermal hysteresis of magnetization and resistivity in $La_{1-x}Sr_xMnO_3$ ($0.5 \leq x \leq 0.6$) with an A-type antiferromagnetic structure. For $0.52 \leq x \leq 0.56$, the magnetization curve exhibits a counterclockwise (CCW) thermal hysteresis about T_N, while the resistivity curve shows a clockwise (CW) thermal hysteresis. On the other hand, samples with $0.58 \leq x \leq 0.6$ exhibit CCW thermal hystereses in both magnetization and resistivity curves. Remarkably, for $x = 0.58$ the rotational direction of thermal hysteresis of resistivity changes from CCW to CW by the magnetic field. This anomalous hysteretic behavior is explained by the competing interaction between the three-dimensional (3D) metallic ferromagnetic and two-dimensional (2D) metallic A-type antiferromagnetic phases.

DOI: 10.1103/PhysRevLett.87.187201 PACS numbers: 75.30.Vn

Colossal magnetoresistance (CMR) found in doped perovskite manganite $La_{1-x}A_xMnO_3$, where A is a divalent ion, has drawn lots of interest due to the possibility of making magnetic devices which utilize this effect [1–5]. Since CMR is mostly observed near the optimal doping range ($x \sim 0.3$), relatively overdoped maganites ($x > 0.5$) have not been extensively studied. However, recent studies on the overdoped samples of $La_{1-x}Sr_xMnO_3$, $La_{1-x}Ca_xMnO_3$, $Nd_{1-x}Sr_xMnO_3$, and $Pr_{1-x}Ca_xMnO_3$ exhibit various unique phenomena related to strong interactions among charge, spin, and lattice degrees of freedom. In particular, the ground states of the half-doped samples such as $La_{0.5}Ca_{0.5}MnO_3$ and $Nd_{0.5}Ca_{0.5}MnO_3$ change from the ferromagnetic (FM) metallic state to an antiferromagnetic (AFM) insulating state, leading to a first order CE-type AFM transition with strong hysteretic behavior in magnetization and resistivity [2,4–7]. Interestingly, T_N is dependent on the thermal cycle. Namely, the FM-to-AFM transition temperature upon cooling is lower than the AFM-to-FM one while warming. Moreover, the FM state shows larger magnitude of magnetization than the AFM phase. Upon cooling and warming the magnitude of the magnetization thus undergoes a large-small-large progression, which typically follows a counterclockwise (CCW) thermal hysteresis as shown in Fig. 1(a). On the other hand, the clockwise (CW) thermal hysteresis is also possible, when the magnitude change accompanies a small-large-small process upon cooling and warming given in Fig. 1(b). In general, the resistivity of half-doped manganites such as $La_{0.5}Ca_{0.5}MnO_3$ and $Nd_{0.5}Ca_{0.5}MnO_3$ has shown a CW thermal hysteresis because the FM phase at higher temperature is more conductive than the CE-type AFM state at lower temperature.

In the Sr-doped manganites $La_{1-x}Sr_xMnO_3$, a CE-type AFM state at $x = 0.5$ has not been observed. Instead, a crossover of ground state from a FM to a type-A AFM state with $d_{x^2-y^2}$ orbital ordering is found around $x \sim 0.52$ [8–12]. The type-A AFM spin structure has a layered arrangement where FM and AFM couplings are present in the ab plane and along the c axis, respectively. Therefore, the 2D metallic state expects to occur in the ab plane. The overdoped manganites $La_{1-x}Sr_xMnO_3$ ($0.5 \leq x \leq 0.6$) have thus been targeted to investigate thermal hysteresis of magnetization and resistivity due to their unique spin structure. The title compounds, which have the first order A-type AFM transition, show an anomalous thermal hysteric behavior in that the rotational direction of the thermal hysteresis is reversed by the doping ratio x or the external magnetic field. Thus far, such an anomalous direction reversal has not been observed in other manganite systems. We are convinced that this unique behavior is strongly correlated with the A-type spin ordering. This Letter presents the thermal hystereses of magnetization and resistivity of $La_{1-x}Sr_xMnO_3$ and compares their thermal hysteretic properties with those of $Nd_{1-x}Sr_xMnO_3$ that also have the A-type AFM structure. We discuss the anomalous thermal hysteresis in terms of the competition between the 3D-metallic FM phase and the 2D-metallic type-A AFM state.

Polycrystalline samples of $La_{1-x}Sr_xMnO_3$ ($0.5 \leq x \leq 0.6$) and $Nd_{1-x}Sr_xMnO_3$ ($x = 0.52, 0.58$) were prepared through the conventional solid-state reaction method. The samples were sintered at 1550 °C for 72 h in air with intermediate grindings, which were then annealed at 1400 °C for 48 h under the O_2 atmosphere to saturate the oxygen site. The resulting samples were thoroughly

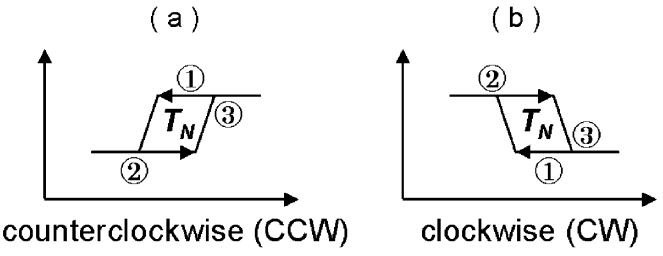

FIG. 1. Schematic diagram of two thermal hysteretic processes which follow the cooling and warming sequence. The magnitude of the (a) counterclockwise (CCW) type undergoes a large-small-large process while that of the (b) clockwise (CW) procedure experiences a small-large-small change.

characterized using x-ray powder diffraction and energy dispersive spectroscopy/scanning electron microscopy techniques, clearly showing that the samples are single phase and maintain their nominal compositions. All the transport measurements were carried out using the standard four probe technique during the cooling and warming sequence. The magnetization data were collected with a commercial SQUID magnetometer.

The temperature dependent magnetization of $La_{1-x}Sr_xMnO_3$ $(0.5 \leq x \leq 0.6)$ measured at 0.5 T for field-cooled (FC) condition is presented in Fig. 2(a). The zero-field resistivity $\rho(T)$ was measured in zero-field-cooled (ZFC) condition. For $x = 0.5$, the paramagnetic (PM) to FM and the insulating to metallic transitions simultaneously occur around $T_C \sim 330$ K. The metallic FM state is stable at low temperature regime. With increasing x, however, T_C is continuously lowered and the metallic FM state becomes unstable. For $0.52 \leq x \leq 0.56$, upon cooling the system undergoes an insulating PM to metallic FM transition in the temperature range of 260 to 310 K. Further decrease of temperature makes the FM magnetization disappear and leads to an abrupt increase in the resistivity. As a result, the system becomes an insulating A-type AFM state in low temperature [8–12]. For $0.58 \leq x \leq 0.60$, the $M(T)$ curves do not show any metallic FM transition but display a PM to AFM transition at $T_N \sim 240$ K, which is in good agreement with a small downturn in the $\rho(T)$ curve. As seen in Fig. 2, $\rho(T)$ curves show the upturn and downturn features around T_N for $0.52 \leq x \leq 0.56$ and $0.58 \leq x \leq 0.6$, respectively.

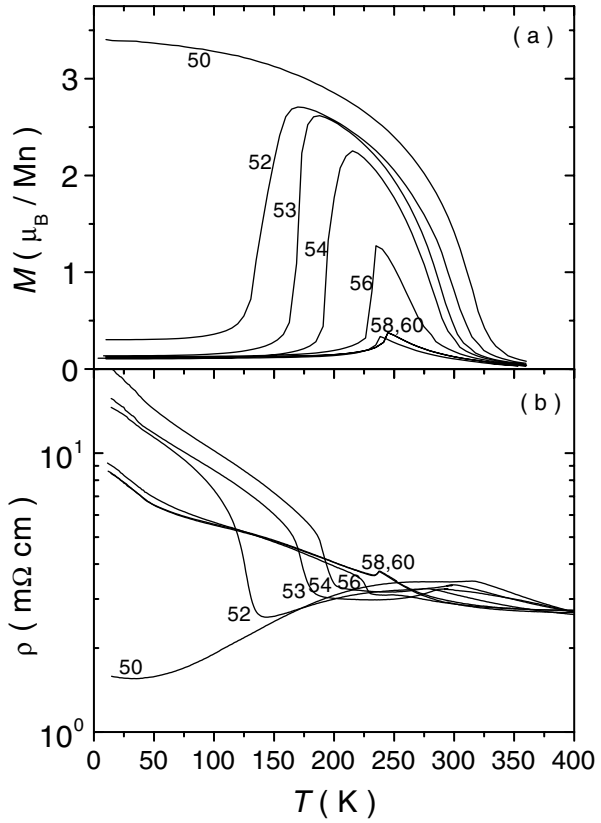

FIG. 2. The (a) magnetization and (b) resistivity for $La_{1-x}Sr_xMnO_3$ as a function of temperature at various doping concentrations where numbers near the curves represent the dopant percentages. Magnetization was measured at 0.5 T after field cooling down to 10 K in 0.5 T. Their temperature-dependent resistivity data were collected under zero field. Only the curves upon warming are displayed for clarity.

To further elucidate the nature of the anomalous thermal hysteresis, we have investigated magnetic and transport properties of two representative samples of $x = 0.53$ and $x = 0.58$ selected from $0.52 \leq x \leq 0.56$ and $0.58 \leq x \leq 0.6$. The $M(T)$ and $\rho(T)$ curves for $x = 0.53$ and 0.58, measured upon cooling and warming, are illustrated in Fig. 3. The temperature dependent magnetization was measured at 0.5 T and the corresponding resistivity was recorded at 0, 3.5, and 7 T. Both $M(T)$ curves show an abrupt drop around T_N and also a hysteretic behavior, suggesting that the transitions to and from an A-type AFM state are first order. However, in $x = 0.53$ the FM-AFM-FM transition occurs in the cooling and warming process while $x = 0.58$ endures the PM-AFM-PM transition. In both cases, the AFM transition temperature upon cooling (T_{NC}) is lower than that upon warming (T_{NW}) and the magnetization magnitude of the FM or PM state at high temperature is larger than that of the AFM state at low temperature. Therefore, both $M(T)$ curves show a CCW thermal hysteresis given in Fig. 1(a).

Figures 3(c) and 3(d) display $\rho(T)$ of $x = 0.53$ and 0.58, respectively, illustrating the rotational direction of thermal hysteresis with and without magnetic field. For $x = 0.53$, the resistivity in the FM region slightly decreases with decreasing temperature. Below 175 K that corresponds to T_N, an abrupt increase of $\rho(T)$ is observed. The upturn temperatures upon cooling and warming agree well with T_{NC} and T_{NW} in the $M(T)$ curves, respectively. The resistivity while cooling near T_N is lower than that upon warming, which is ascribed to the fraction of the FM

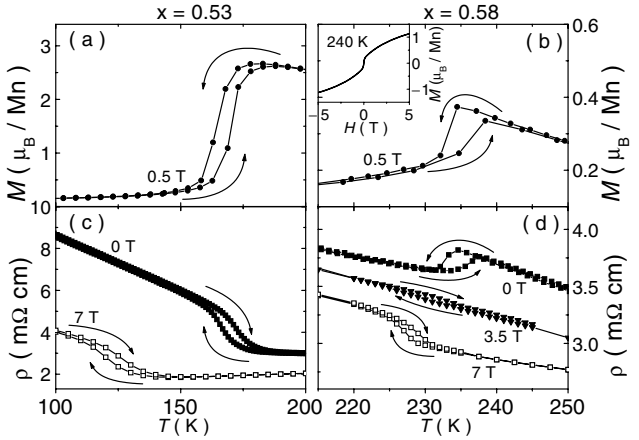

FIG. 3. The temperature dependence of magnetization and resistivity for $x = 0.53$ (left panel) and $x = 0.58$ (right panel). The inset shows the M vesus H curves of $x = 0.58$ at 240 K.

metallic phase. As can be clearly seen in the $M(T)$ curve of Fig. 3(a), the magnitude of magnetization near T_N upon cooling is larger than that while warming. Consequently, $\rho(T)$ for $x = 0.53$ shows a CW thermal hysteresis while cooling and warming. A noticeable feature is that at 7 T the position of the thermal hysteresis shifts to lower temperature but its rotational direction is unchanged.

On the other hand, the zero field resistivity for $x = 0.58$ shows a sudden drop near T_N. This resitivity downturn at T_N appears to be attributed to the phase change from the insulating PM state to the 2D-metallic A-type AFM state [8–12]. As a result, the rotational direction of thermal hysteresis shows a CCW type, which is contrary to that of $x = 0.53$ shown in Fig. 3(c). This discrepancy is presumably due to the difference in the magnetic state above T_N. Namely, the A-type AFM transition in $x = 0.58$ is correlated with an insulating PM state while that in $x = 0.53$ is preceded by a metallic FM phase. A more remarkable feature is that the rotational direction of $x = 0.58$, given in Fig. 3(d), is changed from CCW to CW by the external magnetic field.

Although the origins of the CCW thermal hysteresis and the direction reversal of the thermal hysteresis in the $\rho(T)$ curves by the magnetic field are not clear at this stage, a plausible cause is the coexistence and the competition between the 2D-metallic A-type AFM and the 3D-metallic FM interactions. The inset of Fig. 3(b) displays the $M(H)$ curve of $x = 0.58$ at 240 K. The $M(T)$ curve does not show any clear FM signature near T_N but shows only a PM-to-AFM transition feature. Nevertheless, the $M(H)$ curve above T_N shows a weak FM signature, which is a fast increase of the magnetization at low field region (<0.5 T). This result supports that the 3D-metallic FM interaction coexists and competes with the 2D-metallic A-type AFM interaction. In general, the application of the external magnetic field enhances the 3D-metallic FM interaction but suppresses the 2D-metallic A-type AFM one. As seen in the inset of Fig. 3(b), the percentage of the theoretical saturation magnetization increases from about 10% at 0.5 T to about 27% at 3.5 T. The percentage of the 3D-metallic FM state above 3.5 T is larger than the 3D percolation threshold of 10%–25% [13,14]. It is conceivable that the magnetic field can induce a percolation pathway between the 3D-metallic FM regions, which is accompanied by the change from the downturn anomaly to the upturn one in the $\rho(T)$ curve upon cooling. We thus conjecture that the anomalous thermal hysteric behavior with the change of x or the magnetic field is closely correlated with the percolation phenomenon.

Taken together, we have constructed the phase diagram of $La_{1-x}Sr_xMnO_3$ as a function of T and x, which is given in Fig. 4. Three principal regions are divided: an insulating PM state, a metallic FM one, and a 2D-metallic A-type AFM one in which the resistivity lies in between metallic and insulating states. In this phase diagram, the curved solid lines that separate each region are made by connecting T_C (solid square), T_{NC} (solid circle), and T_{NW} (open circle) at specific doping concentration. The dense dotted region between T_{NC} and T_{NW} corresponds to the temperature range showing thermal hysteresis. The hatched regime indicates the approximate FM boundary induced by the application of magnetic field. Since the external field enhances the FM double exchange interaction, it increases T_C and decreases T_N. We also include the spin structure of each magnetic state based on the neutron experimental result [8,9].

Now, we turn to the relative magnitude of the magnetization at the phase boundary near T_N within the framework of double exchange theory. The FM and PM magnetization abruptly decreases at T_N, suggesting that the magnetization magnitude around T_N reduces in order of the FM, PM, and AFM state. Thus, the relative magnetization values of the FM, PM, and AFM states near T_N can be assigned as M_{large}, M_{middle}, and M_{small}, respectively. In a similar way, we denoted the relative magnitude of the resistivity in the three distinctive phases where the FM metallic and PM insulating states are assigned to ρ_{small} and ρ_{large}, respectively. In the A-type AFM state, it is conceivable that the system gains the maximum kinetic energy via e_g electron hoping when the $d_{x^2-y^2}$ orbital forms a pseudo–2D band [8,9]. In this context, the A-type AFM phase can be viewed as a 2D metallic state induced by the in-plane FM double exchange interaction. Relatively, the resistivity of the A-type AFM state should lie in between the FM and PM states, which is thus assigned as ρ_{middle}. In boxes lined with dashed marks, we summarized the relative magnitude of magnetization and resistivity near T_N.

The results regarding the type of thermal hysteresis in $La_{1-x}Sr_xMnO_3$ are well matched with the phase diagram. For $0.52 \leq x \leq 0.56$, the change of the magnetization around T_N while cooling and warming is in order of $M_{large} - M_{small} - M_{large}$, which corresponds to the

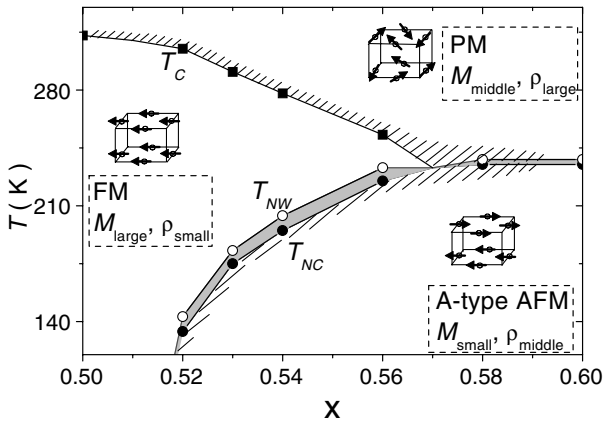

FIG. 4. Phase diagram of temperature versus doping concentration for $La_{1-x}Sr_xMnO_3$ ($0.5 \leq x \leq 0.6$). The dense dotted region between T_{NW} and T_{NC} indicates the temperature range where thermal hystereses are observed in the magnetization and resistivity data. The hatched regime represents the FM state that can be extended by an applied magnetic field. The relative magnitudes of magnetization and resistivity in PM, FM, and A-type AFM states near T_N are displayed in dashed line boxes.

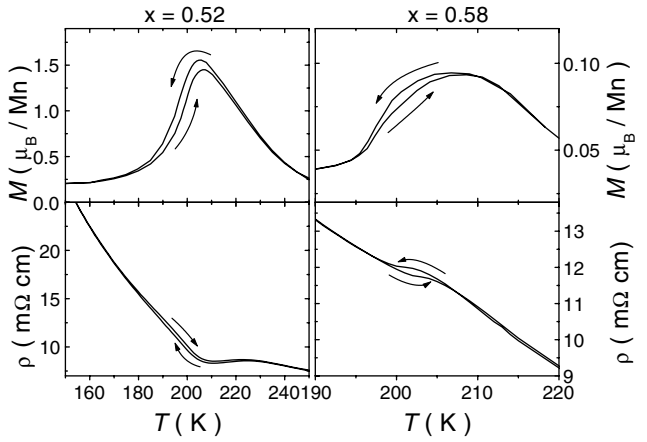

FIG. 5. The temperature dependence of magnetization and zero-field resistivity for $x = 0.52$ (left panel) and $x = 0.58$ (right panel) in $Nd_{1-x}Sr_xMnO_3$. Magnetization measurements were carried out at 0.5 T.

CCW type shown in Fig. 1(a). Whereas, $\rho(T)$ follows the $\rho_{\text{small}} - \rho_{\text{middle}} - \rho_{\text{small}}$ process that is consistent with the CW cycle given in Fig 1(b). For $0.58 \leq x \leq 0.60$, the magnetization magnitude near T_N upon cooling and warming follows the $M_{\text{middle}} - M_{\text{small}} - M_{\text{middle}}$ pathway, which is thus considered as the CCW type. The resistivity value changes in the order of $\rho_{\text{large}} - \rho_{\text{middle}} - \rho_{\text{large}}$, which also agrees with the CCW type. In the absence of magnetic field, the 2D-metallic AFM state appears to suppress the 3D-metallic FM state above $x \sim 0.57$. In the presence of the external field, however, the AFM state is suppressed and the FM domain is extended into the PM regime, leading to the creation of the metallic FM phase near T_N such as the Fig. 4 hatched region. The external field thus changes the magnetic state of the system from PM-AFM-PM to FM-AFM-FM near T_N. Namely, the magnetization and resistivity values change from $M_{\text{middle}} - M_{\text{small}} - M_{\text{middle}}$ to $M_{\text{large}} - M_{\text{small}} - M_{\text{large}}$ and from $\rho_{\text{large}} - \rho_{\text{middle}} - \rho_{\text{large}}$ to $\rho_{\text{small}} - \rho_{\text{middle}} - \rho_{\text{small}}$, respectively. As a result, the rotational direction of thermal hysteresis is sustained in $M(T)$ but is inverted in $\rho(T)$.

From the results discussed above, the anomalous thermal hysteresis in $La_{1-x}Sr_xMnO_3$ is mainly attributed to the *A*-type AFM spin structure with the 2D-metallic character. In order to verify this conjecture, we have investigated the thermal hysteresis of $Nd_{1-x}Sr_xMnO_3$ which has a CE-type and an *A*-type spin structure for $x \sim 0.5$ and $0.55 \leq x \leq 0.6$, respectively [6,15]. We collected the magnetization and resistivity data for two representative samples having the compositions of $x = 0.52$ and $x = 0.58$, which are shown in Fig. 5. With increasing x, the suppression of the FM phase in $Nd_{1-x}Sr_xMnO_3$ is more severed than in $La_{1-x}Sr_xMnO_3$. However, the $M(T)$ curves of both compositions show a CCW thermal hysteresis as found in $La_{1-x}Sr_xMnO_3$. With decreasing temperature, the resistivity of $Nd_{1-x}Sr_xMnO_3$ is much larger than that of $La_{1-x}Sr_xMnO_3$. As a consequence, the thermal hysteretic behavior of $Nd_{1-x}Sr_xMnO_3$ is less distinctive in comparison with that of $La_{1-x}Sr_xMnO_3$, but the anomalous feature is still observed in the Nd-doped compounds. The $\rho(T)$ curve of $x = 0.52$ shows an upturn around T_N and a CW thermal hysteresis while $x = 0.58$ exhibits a slight downturn anomaly in the $\rho(T)$ curve near at T_N and a CCW thermal hysteresis. These results are in excellent agreement with those found in $La_{1-x}Sr_xMnO_3$, supporting that the anomalous thermal hysteric behavior is closely related to the 2D-metallic *A*-type AFM state. It is worth noting the undoped manganite $LaMnO_3$ which has the same *A*-type AFM spin structure [3]. However, the resistivity of $LaMnO_3$ is several orders of magnitude larger than that of $La_{1-x}Sr_xMnO_3$ ($0.52 \leq x \leq 0.60$). Consequently, the pseudo 2D-metallic band cannot be realized in $LaMnO_3$, suggesting that it is very difficult to find an anomalous thermal hysteretic behavior in $LaMnO_3$.

In summary, for the first time we have discovered anomalous thermal hysteretic behavior in the overdoped manganites $La_{1-x}Sr_xMnO_3$ with the *A*-type AFM spin structure. More specifically, near T_N increasing doping concentration reversed the rotational direction of thermal hysteresis. Such an anomalous direction reversal is also achieved by applying a magnetic field. From our studies, we are able to claim that these anomalous thermal hysteretic behaviors are largely attributed to the competition between the 3D-metallic FM and the 2D-metallic *A*-type AFM interactions.

We are pleased to acknowledge helpful discussion with J. G. Park. The Creative Research Initiative Program supported this work.

*Corresponding author.
Electronic address: nhhur@kriss.re.kr

[1] C. Zener, Phys. Rev. **82**, 403 (1951).
[2] J. M. D. Coey *et al.,* Adv. Phys. **48**, 167 (1999).
[3] E. O. Wollan and W. C. Koehler, Phys. Rev. **100**, 545 (1955).
[4] P. Schiffer *et al.,* Phys. Rev. Lett. **75**, 3336 (1995).
[5] A. Urushibara *et al.,* Phys. Rev. B **51**, 14 103 (1995).
[6] H. Kawano *et al.,* Phys. Rev. Lett. **78**, 4253 (1997); Physica (Amsterdam) **241B**, 289 (1998).
[7] J. Dho *et al.,* Phys. Rev. B **60**, 14 545 (1999).
[8] T. Akimoto *et al.,* Phys. Rev. B **57**, R5594 (1998).
[9] Y. Morimoto *et al.,* Phys. Rev. B **58**, 5544 (1998).
[10] H. Fujishiro *et al.,* J. Phys. Soc. Jpn. **67**, 2582 (1998).
[11] K. Kikuchi *et al.,* J. Solid State Chem. **146**, 1 (1999).
[12] S. I. Patil *et al.,* J. Appl. Phys. **87**, 5028 (2000); Phys. Rev. B **62**, 9548 (2000).
[13] B. I. Shklovskii and A. L. Efros, *Electronic Properties of Doped Semiconductors* (Springer, New York, 1984).
[14] M. Uehara *et al.,* Nature (London) **399**, 560 (1999).
[15] H. Kuwahara *et al.,* Phys. Rev. Lett. **82**, 4316 (1999).